

Article

The Effect of Void on the Cold Deformation Behaviour of $\alpha_2 + \gamma$ Two Phase Ti-Al Alloy

Ruicheng Feng ^{1,2} , Maomao Wang ¹ 

¹ School of Mechanical and Electronical Engineering, Lanzhou University of Technology, Lanzhou 730050, China; frcly@163.com (R.F.); 15620864891@163.com (M.W.)

² State Key Laboratory of Advanced Processing and Recycling of Non-ferrous Metals, Lanzhou University of Technology, Lanzhou 730050, China

* Correspondence: e-mail@e-mail.com; Tel.: +x-xxx-xxx-xxxx

Version October 9, 2018 submitted to Journal Not Specified

Abstract: Fracture processes of nanocrystalline metallic materia is affected by dislocation, nano void and other defects. Existing studies of defect evolution in titanium-aluminium alloy cover the case that voids located in single crystals, inside grain in poly crystals and at the grain boundaries. Molecular dynamics simulation was performed to study the evolution of a spherical nano void in $\alpha_2 + \gamma$ two-phase titanium-aluminium alloy under uniaxial tension. The results show that voids located at the α_2 / γ phase boundary have significant detract to strength of Ti-Al polycrystalline.

Keywords: $\alpha_2 + \gamma$ two phase TiAl alloy; void; molecular dynamics

1. Introduction

Brittle fracture in Ti-Al alloy strongly affects the safety of fracture of structure like turbo of aircraft engine and combustion generator [1]. Two-phase titanium aluminum alloys with proper phase distribution and grain size exhibit better mechanical performance compared with monolithic constituents $\gamma(\text{TiAl})$ and $\gamma(\text{Ti}_3\text{Al})$ alloy [2]. Deformation phenomena of TiAl alloys have been widely studied in order to overcome the problems associated with the limited ductility and damage tolerance. A great number of literature covers a wide range of parameters such as alloy composition, microstructure and deformation temperature. Much of the work has been performed on single phase γ alloys and PST crystals[3]. Rapture failure at the macroscopic scale can be attributed to nucleation, growth and propagation of cracks, but at the microscopic scale cracks are initially easily formed at defects in the casting process, such as voids and inclusions [4]. The initiation of crack at microscopic scale is a dynamic process, which resulting in difficulties on study of detailed mechanisms of deformation and cracking. These defects are known to play a fundamental role in the deformation of the material. Nucleation, growth and coalescence of voids are deemed as the primary mechanism of ductile material fracture, in which void growth is particularly important [5]. Therefore, it is necessary to study the deformation response of porous materials with the consideration of microstructure evolution.

Defects such as grain boundary, void and segregation plays an significant role in the process of fracture [6]. In order to understanding the mechanism of brittle fracture, multi-scale methods from micro to marco scale have been applied to investigate the behavior of fracture. It's necessary to carefully examine the revolution of defects and its influence on the fracture process at atomic scale. A previous study on void growth in γ -TiAl single crystal has reveals that void with high volume fraction detracts incipient yield strength [4].Molecular dynamics(MD method has been use to investigate the evolution of void in materials in nanoscale [4,7,8]. The fracture mechanisms in the duplex micro-structure are plasticity induced grain boundary decohesion and cleavage, while those in the lamellar micro-structure are interface delamination and cracking across the lamellar [?].

33 MD simulations has reveals that existence of voids alone may contribute to strain hardening
 34 because theyare barriers to dislocation movement [9]

35 2. Molecular Dynamics Simulation

36 2.1. Atomic Potential

37 The interaction of particle in the material is determined by interatomic potential. Many reported
 38 examples of crack propagation in metal materials were performed with embedded atomic method
 39 due to is better accuracy in metal lattice compare with F-S and L/J [10]. The embedded atom method
 40 (MEAM) potential developed by Zope and Mishin [11] was used in the study. The simulation is
 41 submitted by MD simulations with the Large-scale Atomic/Molecular Massively Parallel Simulator
 42 (LAMMPS) open-source code [12]. We performed constant-pressure and constant-temperature (NPT)
 43 molecular dynamics simulation. The definitnion of potential is as following:

$$E_{total} = \sum_i F_i(\rho_{h,i}) + \frac{1}{2} \sum_i \sum_{j(j \neq i)} \phi_{ij}(R_{ij}) \quad (1)$$

44 where E_{total} is the total energy of the system, $\rho_{h,i}$ is the host electron density at atom i due to the
 45 remaining atoms of the system, $F_i(\rho)$ is the energy for embedding atom i into the background electron
 46 density ρ , and $\phi_{ij}(R_{ij})$ is the core-core pair repulsion between atoms i and j separated by the distance
 47 R_{ij} . It can be noted that F_i only depends on the element of atom i and ϕ_{ij} only depends on the elements
 48 of atoms i and j . The electron density is, as stated above, approximated by the superposition of atomic
 49 densities.

50 2.2. Model Creation of Crystalline

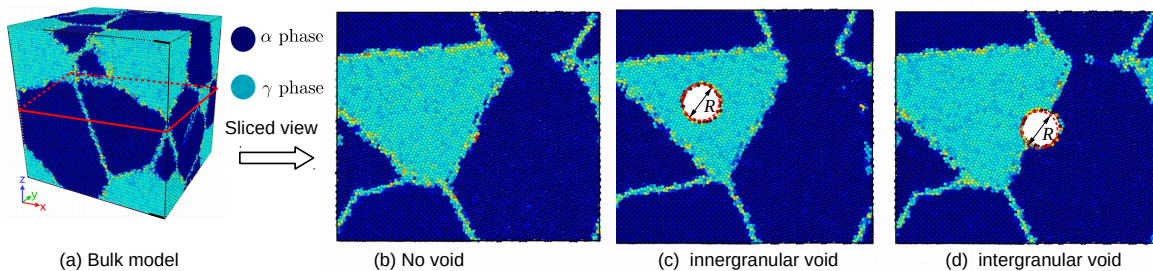


Figure 1. Overview of model creation

51 γ TiAl has a fcc-centered tetragonal with an $L1_0$ structure, and α_2 – TiAl is hcp structure, the
 52 structure of the two initial cells are shown in Fig.??, and the constructing parameters are givin by Table.
 53 1. The simulation cells of two phase polycrystalline with an initially spherical void at different position
 54 are shown in figure []. Periodic boundary conditions (PBC)are applied along all three directions,
 55 that makes poly crystal with periodic nanovoid structures. The initial dimension of simulation cell
 56 is $L_x = 20$ nm, $L_y = 18$ nm, $L_z = 21$ nm, and each model contains about 4.6 million atoms. The
 57 grain orientation and size were randomly created with Voronoi method with code ATOMSK [], and
 58 resulting in the arbitrary shape and orientation of the grains. Only one spherical void defect was placed
 59 intragranularlly or intergranularlly within each simulation model void within each simulation model.
 60 The intragranular spherical void was located in grain interior of the largest grain of the simulation
 61 model, as shown in Fig. []. The intergranular spherical void was at the center of the simulation cell, as
 62 shown in Fig. [].

63 2.3. Analysis method

64 The centrosymmetry parameter is defined as follow:

Table 1. Parameters of nanocrystalline

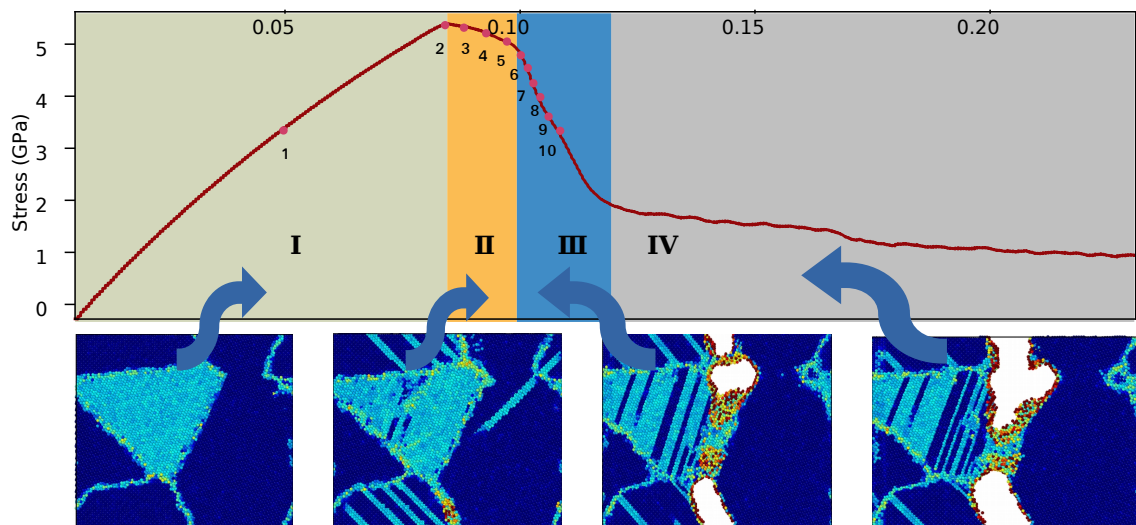
Phase	Space group	Designation	Parameters
α_2	P6 ₃ /mmc	0 ₁₉	$a = 0.5765$ $c = 0.46833$
γ	tP4	L1 ₀	$a = 0.3997$ $c = 0.4062$

$$P = \sum_{i=1}^6 |\vec{R}_i + \vec{R}_{i+6}|^2 \quad (2)$$

where \vec{R}_i and \vec{R}_{i+6} are the vectors corresponding to the six pairs of opposite nearest neighbors in the fcc lattice. The centrosymmetry parameter(CSP) is zero for atoms in a perfect lattice. In other words, if the lattice is distorted the value of P will not be zero. Instead, the parameter will have a value within the range corresponding to a particular defect. By removing all the perfect and surface atoms within the bulk, the existence of dislocation atoms become visible.

3. Results and Discussion

In order to examine deformation behaviour carefully, tensile loading was applied to the model without any types of void defect. The whole tension process was separated into four stages: Stage-1 is typical elastic part of the deformation, which is originated from $\epsilon = 0$ to $\epsilon = 0.092$, including key point 1. Stage-2 is yield stage ranging from $\epsilon = 0.092$ to $\epsilon = 0.101$, including key points 2 to 6. In stage-2, the stress decreased slightly along with the increasing of strain. Stage-3 is cracking stage and in this stage the strength of the model have been was detracted sharply, we can confine that the structure almost fail after the stage-3. Snapshots of atoms configuration are labeled with key points number from 1 to 10, specific list of key points numbers were shown in Table.2. Deformation behaviour of the α_2 phase had γ phase were discussed in the following subsection respectively.

**Figure 2.** Deformation process of the model without void defect**Table 2.** Key point during tensile process

Key Number	1	2	3	4	5	6	7	8	9	10
Time/ps	0	0.15	0.16	0.17	0.18	0.19	0.20	0.21	0.22	0.23
Strain	0	0.092	0.094	0.096	0.099	0.101	0.104	0.107	0.110	0.112

80 3.1. Deformation Behaviour of Two Phase Alloys without Void Defects

81 However, the following discussion concentrates on deformation phenomena that rely on the
 82 elastoplastic codeformation of the γ and α_2 phases and on the particular point defect situation occurring
 83 in twophase alloys. Due to this effect ($\alpha_2 + \gamma$) alloys exhibit some remarkable properties that are
 84 unlike those of either constituent.

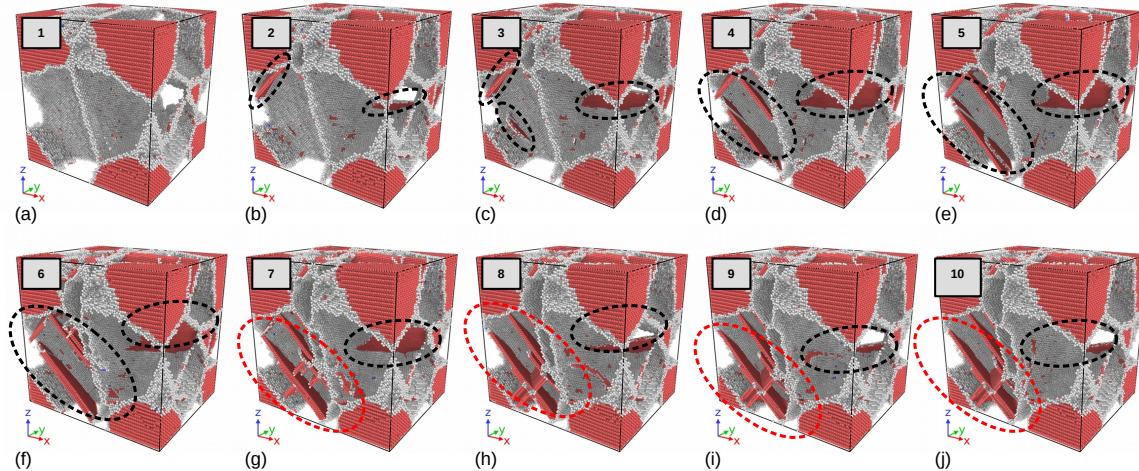


Figure 3. Defect evolution in γ phase (perfect atoms of α phase have been removed)

85 The configure of atoms is shown in Fig.7, it can be seen that disilication emission initiate in γ
 86 pahse in XXX ps, and the deformation canbe mainly confied to the majority γ pahse. γ (TiAl) deforms
 87 by octahedral glide of ordinary dislocations with the Burgers vector $b=1/2<110]$ and superdislocations
 88 with the Burgers vectors $b = <101]$ and $b = 1/2 < 11\bar{2}]$. The other potential deformation mode is
 89 mechanical twinning along $1/6 < 11\bar{2}111$.

90 From Fig.7, of the two constituents of $(\alpha_2+\gamma)$ alloys, the α_2 phase is more difficult to deform.
 91 A reason for the unequal strain partitioning between the α_2 and γ phase is certainly the strong
 92 plastic anisotropy of the α_2 phase. TEM examinations performed on tensile tested lamellar alloys
 93 have revealed that the limited plasticity of the α_2 phase is mainly carried by local slip of $<\mathbf{a}>$ -type
 94 dislocations with the Burgers vector $b = 1/3 < 11\bar{2}0 >$ prism planes⁷, which is by far the easiest slip
 95 system in α_2 single crystals.

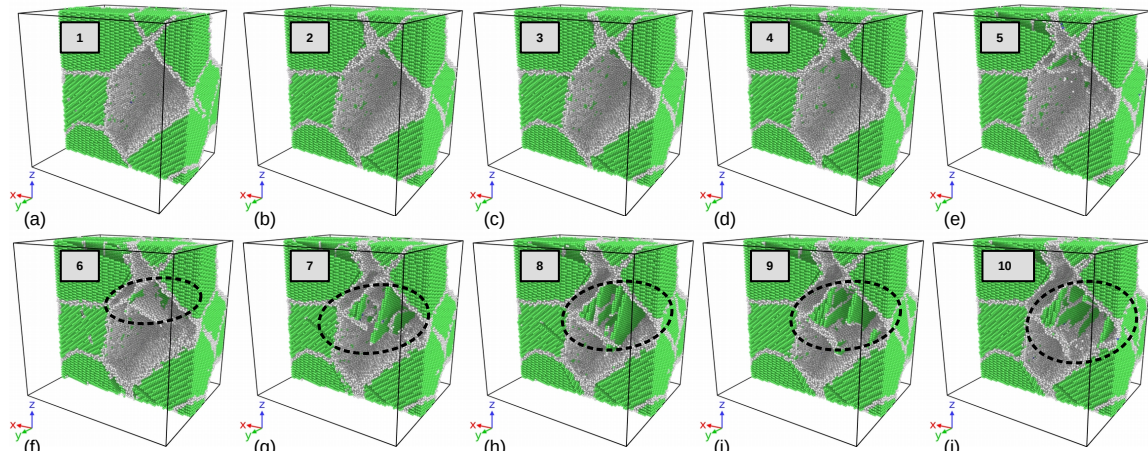


Figure 4. Defect evolution in α_2 -phase (perfect atoms in α_2 phase have been removed)

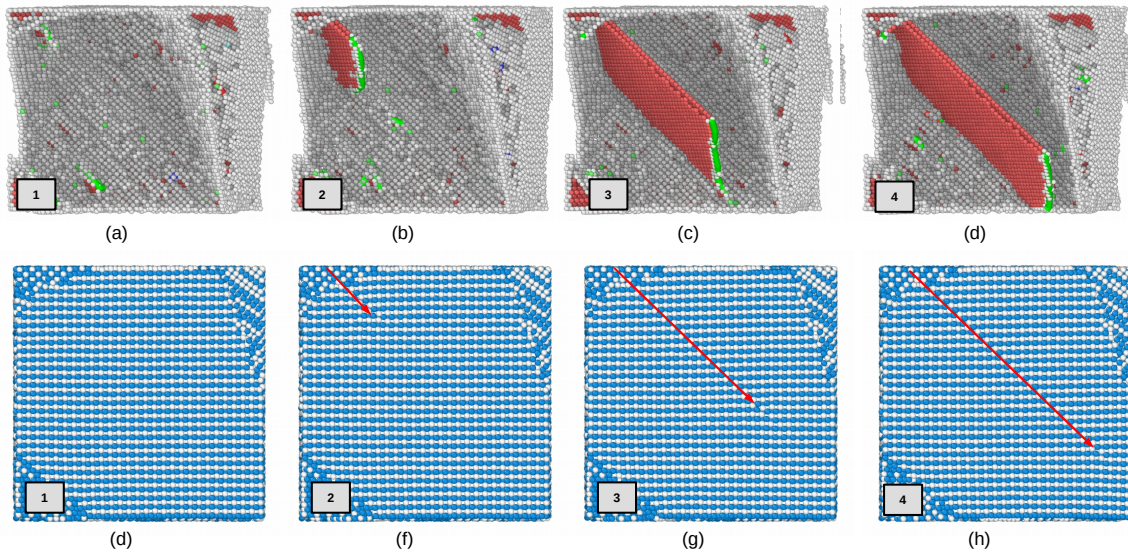


Figure 5. Dislocation in γ

96 In many cases the orientation of slip slip is changed because the crystallographically available
 97 slip and directions are not continuous across the interface. This may significantly reduce the Schmid
 98 factor and thus impede slip transfer. At the γ/γ interfaces the orientation of the slip plan could change
 99 through a relevantly large angle of about 90 degree. Reorientation of slip is always required at the
 100 α_2/γ interface; the smallest angle between the corresponding slip planes 111_γ and $10 - 10_{\alpha_2}$ is about
 101 19 degree [1].

102 The core of a dislocation intersecting an interface often needs to be transformed. For example,
 103 an ordinary $1/2<110]$ dislocation gliding in one γ grain has to be converted in to a $<101]$ super
 104 dislocation with the double Burgers vector gliding in an adjacent γ grain. At the α_2/γ interface the
 105 dislocations existing in the $D0_{19}$ structure have to be transformed into dislocations consistent with the
 106 $L1_0$ structure. These core transformations are associated with a change of the dislocation line energy
 107 because the lengths of the Burgers vectors and the shear module are different.

108 Dislocations crossing semi-coherent boundaries have to intersect the misfit dislocations, a process
 109 that involves elastic interaction, jog formation and the incorporation of gliding dislocations into the
 110 mismatch structure of the interface. When the slip is forced to cross α_2 lamella, pyramidal slip of the α_2
 111 phase is required, which needs an extremely high shear stress.

112 3.2. Evolution of spherical void in the simulation with intragranular spherical voids

The volume defects considered pertain to three-dimensional objects contained within a matrix. Three-dimensional structures composed of zero-, one- or two-dimensional defects are not considered here. Second-phase particles, precipitated within, as a consequence of a thermal treatment, or taken up, as a consequence of a material processing route, into a matrix of the first, dominant phase, disrupt, more or less (as possibly associated with the occurrence of incoherent or coherent interfaces; see Sect. 5.3), the long-range translation symmetry of the matrix. They may induce considerable misfit-stress fields and thus can influence material properties pronouncedly. Such stress fields surrounding the second-phase particles can be due to misfit between the volume occupied by the second-phase particle when unconstrained and the space ("hole") put at its disposal by the matrix. Such misfit can arise due to specific volume differences induced by precipitation or by different thermal expansion or shrinkage upon heating or cooling the specimen. A possibly favorable effect of second-phase particles is a contribution to the enhancement of mechanical strength. Considering yielding of a material as related to glide of dislocations (Sect. 5.2.5), any mechanism obstructing dislocation glide improves the mechanical strength. In the discussion of the Frank–Read source for dislocation (-line) production (Sect.

5.2.6) it was made clear that second-phase particles can serve as obstacles for dislocation migration: the stress fields surrounding the second-phase particles can be of “antagonistic” nature and “block” propagation of the stress field of a migrating dislocation: the second-phase particle acts as “pinning point”. It was already indicated that in order that a dislocation can pass two pinning points (A and B in Fig. 5.13; see Sect. 5.2.6) a critical shear stress is needed that depends on the distance between the obstacles (which can be second-phase particles):

$$\tau_0 = Gb/d \quad (3)$$

where d represents the distance between A and B and thus reflects the dependence of the critical shear stress τ_0 on the second-phase particle density and distribution. This mechanism for hardening is designated as the Orowan process (with τ_0 as the Orowan (shear) stress ; sgtee also Sect. 11.14.4). As a result of the Orowan process, upon passage of the pinning points by a series of gliding dislocations, a system of concentric loops is formed around the second-phase particles (see Fig. 5.27). Consequently, the effective average distance between the second-phase particles has decreased to d which implies a necessary increase of the value of critical shear stress required for continuation of dislocation glide (cf. (5.10)). A step, of the width of a burgers vector, will be generated at both sides of a crystal along the direction of the burgers vector after dislocation traversing the entire crystal, as is shown in ???. A small step will be formed at spherical void surface toward the void interior after dislocation absorption at spherical void surfaces, as is shown in ???. If a great number of dislocation slip along their respective systems towards the spherical nano void in all directions, and are absorbed at the spherical void surfaces, the spherical nano void will eventually shrink from the dash circle to

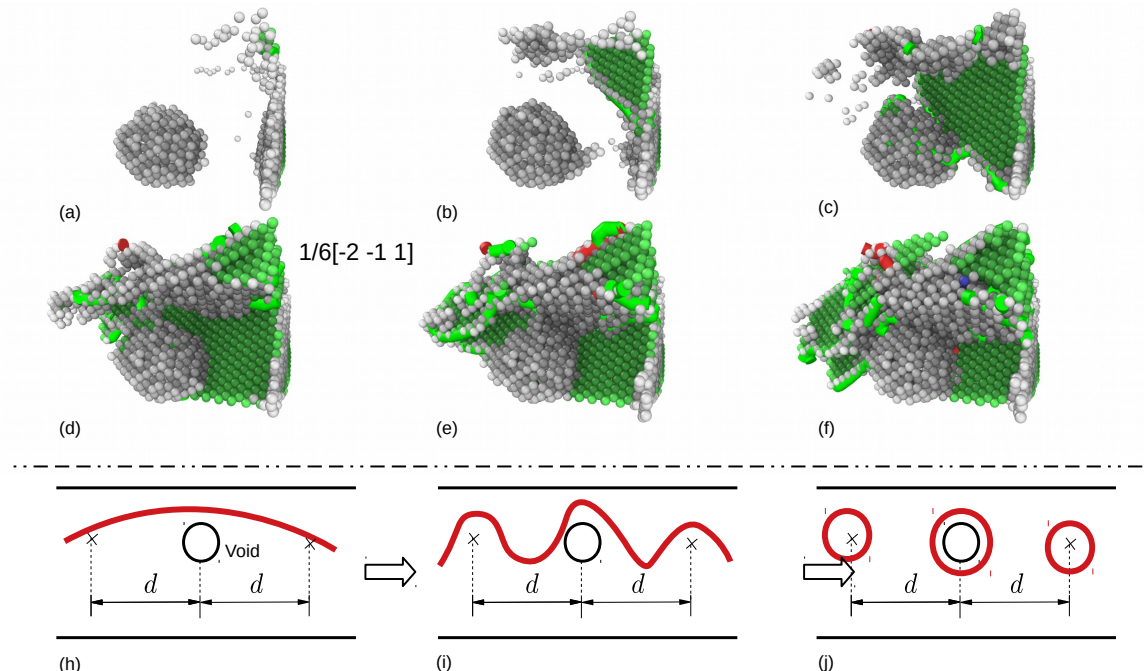


Figure 6. Orowan process in α -phase (α phase atoms have been removed)

3.3. The effect of void on the strength of material

Void of $R=10 \text{ \AA}$ was placed at phase boundary, inside α_2 phase grain respectively. Effect of void at different position under uniaxial tension is shown in Fig.8. The strength of materials with void in different size and at different position is shown in Fig.8. The results show that the model without void defect has best strength, while the void located inside α_2 phase detracts the strength of the material most, and the void at phase boundary have less impact on the strength.

132 The effect of size is expectable that the greater voids detracts the strength of the materials more,
 133 however, it has been observed in the simulation that there is a critical value about 15A for voids at
 134 different position. The voids larger than 15 A have dramatic detraction to the strength of the material.
 135 Conventional definition of strength of materials with geometry subtraction was applied to the model,
 136 and theoretical strength of the models was calculated by formulation 4:

$$\sigma^* = \sigma_0 \cdot \frac{A^*}{A_0} \quad (4)$$

137 where σ_0 is the strength of the model without void defects 5.26 Gpa, and A_0 is initial section
 138 area, $A = 36000AA^2$, A^* is section area in consider of the subsection that results from the voids.
 139 Comparing with the strength determined by molecular dynamics simulation and the results calculated
 140 with formulation 4, it can be assumed that the main factor that affects the strength of materials can be
 141 attributed to local behaviour of the materials, thus revolution of defects should be examined carefully.

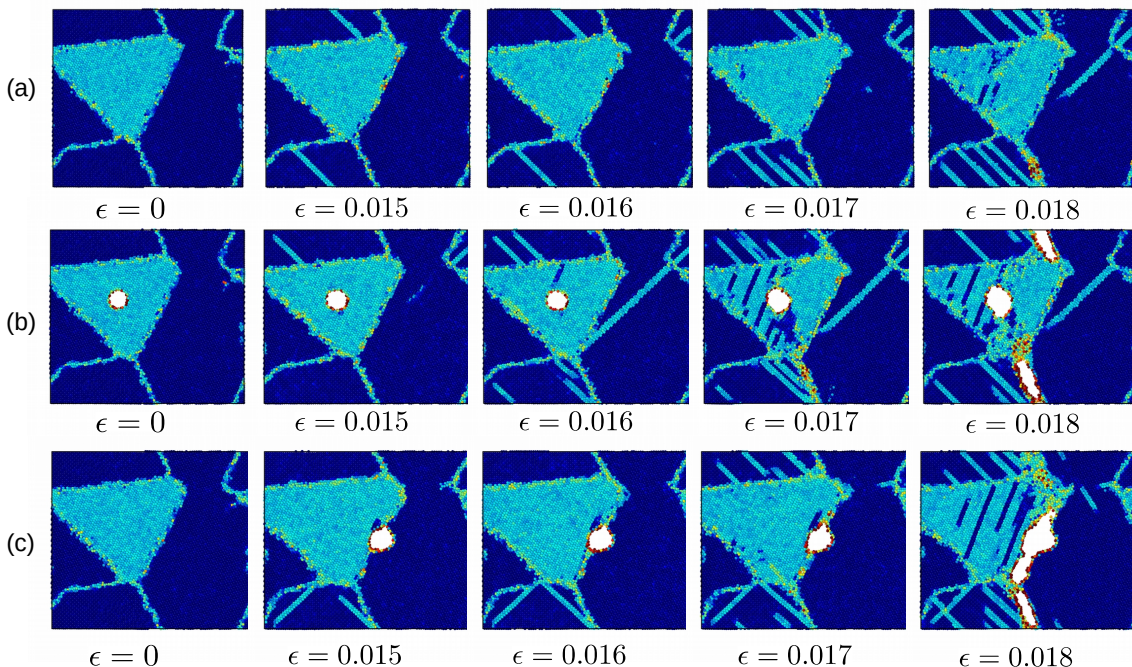


Figure 7. Yield process of the models

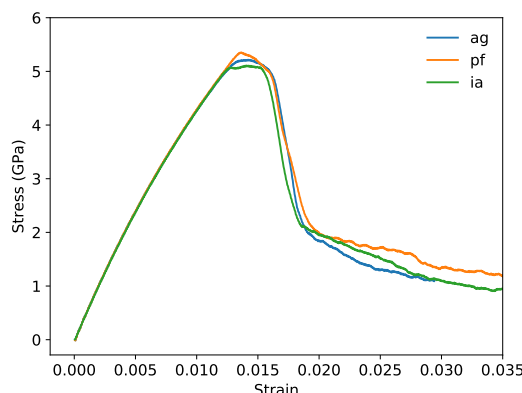


Figure 8. Stress-Strain

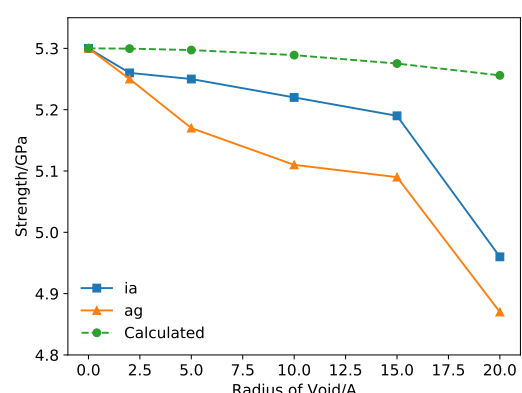


Figure 9. Strength of models

Voids with different size: 2A, 5A, 10A, 15A were placed into the model respectively. It has been observed that voids detracts the strengths of the material. The max stress stress of the simulation cell decreases as the volume of voids are larger. From Fig ??, there is a critical value of void radius about 15A, the void greater than 15A cause serious detraction of strength of material. Engineering stress is calculated

$$\sigma = S/A$$

¹⁴² The rate of decrease of loading area are smaller comparing with the detraction of strength, so it can
¹⁴³ be assumed that the yield behaviour and strength is much more related with local behaviour of
¹⁴⁴ grain boundaries and void.

¹⁴⁵ Grain and phase boundaries are obstacles to deformation process, thus the stability of boundaries
¹⁴⁶ have great impact on the strength of materials. Interaction between grainboundary and void determines
¹⁴⁷ the fracture mode of the TiAl alloy.

According to Schmid's law:

$$\tau = \sigma * m$$

where m is the Schmid factor :

$$m = \cos(\phi)\cos(\lambda)$$

¹⁴⁸ References

- ¹⁴⁹ 1. Munz, E.D. Psychotherapie in der Psychiatrie. *Nervenheilkunde* **2017**, *36*, 800–805, [[arXiv:1011.1669v3](#)].
¹⁵⁰ doi:10.1007/s13398-014-0173-7.2.
- ¹⁵¹ 2. Kim, Y.W. Effects of microstructure on the deformation and fracture of γ -TiAl alloys. *Materials Science and*
¹⁵² *Engineering: A* **1995**, *192-193*, 519–533. doi:10.1016/0921-5093(94)03271-8.
- ¹⁵³ 3. Appel, F.; Clemens, H.; Fischer, F.D. Modeling concepts for intermetallic titanium aluminides. *Progress in*
¹⁵⁴ *Materials Science* **2016**, *81*, 55–124. doi:10.1016/j.pmatsci.2016.01.001.
- ¹⁵⁵ 4. Tang, F.L.; Cai, H.M.; Bao, H.W.; Xue, H.T.; Lu, W.J.; Zhu, L.; Rui, Z.Y. Molecular dynamics
¹⁵⁶ simulations of void growth in γ -TiAl single crystal. *Computational Materials Science* **2014**, *84*, 232–237.
¹⁵⁷ doi:10.1016/j.commatsci.2013.12.014.
- ¹⁵⁸ 5. Hempel, N.; Bunn, J.R.; Nitschke-Pagel, T.; Payzant, E.A.; Dilger, K. Study on the residual stress relaxation
¹⁵⁹ in girth-welded steel pipes under bending load using diffraction methods. *Materials Science and Engineering*
¹⁶⁰ *A* **2017**, *688*, 289–300. doi:10.1016/j.msea.2017.02.005.
- ¹⁶¹ 6. Larsen, P.M.; Schmidt, J. Robust structural identification via polyhedral template matching.
¹⁶² *Modelling and Simulation in Materials Science and Engineering* **2016**, *24*, 055007, [[\[1603.05143\]](#)].
¹⁶³ doi:10.1088/0965-0393/24/5/055007.
- ¹⁶⁴ 7. Jing, P.; Yuan, L.; Shivpuri, R.; Xu, C.; Zhang, Y.; Shan, D.; Guo, B. Evolution of spherical nanovoids within
¹⁶⁵ copper polycrystals during plastic straining: Atomistic investigation. *International Journal of Plasticity* **2018**,
¹⁶⁶ *100*, 122–141. doi:10.1016/j.ijplas.2017.09.016.
- ¹⁶⁷ 8. Elkhatib, M.G.; Shin, Y.C. Molecular dynamics-based cohesive zone representation of Ti6Al4V/TiC
¹⁶⁸ composite interface. *Materials and Design* **2018**, *155*, 161–169. doi:10.1016/j.matdes.2018.05.054.
- ¹⁶⁹ 9. Xiong, L.; Xu, S.; McDowell, D.L.; Chen, Y. Concurrent atomistic-continuum simulations of dislocation-void
¹⁷⁰ interactions in fcc crystals. *International Journal of Plasticity* **2015**, *65*, 33–42. doi:10.1016/j.ijplas.2014.08.002.
- ¹⁷¹ 10. Ko, W.S.; Grabowski, B.; Neugebauer, J. Development and application of a Ni-Ti interatomic potential
¹⁷² with high predictive accuracy of the martensitic phase transition. *Physical Review B* **2015**, *92*, 134107.
¹⁷³ doi:10.1103/PhysRevB.92.134107.
- ¹⁷⁴ 11. Zope, R.R.; Mishin, Y. Interatomic potentials for atomistic simulations of the Ti-Al system.
¹⁷⁵ *Physical Review B - Condensed Matter and Materials Physics* **2003**, *68*, 024102, [[\[arXiv:cond-mat/0306298\]](#)].
¹⁷⁶ doi:10.1103/PhysRevB.68.024102.
- ¹⁷⁷ 12. Plimpton, S. Fast parallel algorithms for short-range molecular dynamics. *Journal of Computational Physics*
¹⁷⁸ **1995**, *117*, 1–19, [[\[arXiv:10.1002/nag.2347\]](#)]. doi:10.1006/jcph.1995.1039.

¹⁷⁹ © 2018 by the authors. Submitted to *Journal Not Specified* for possible open access
¹⁸⁰ publication under the terms and conditions of the Creative Commons Attribution (CC BY) license
¹⁸¹ (<http://creativecommons.org/licenses/by/4.0/>).